A R C H I V E S O F M E T A L L U R G Y A N D M A T E R I A L S
Volume 56 2011 Issue 2
DOI: 10.2478/v10172-011-0055-3

K. KOWALCZYK-GAJEWSKA*

MICROMECHANICAL MODEL OF POLYCRYSTALLINE MATERIALS WITH LAMELLAR SUBSTRUCTURE

MIKROMECHANICZNY MODEL MATERIAŁÓW POLIKRYSTALICZNYCH O SUBSTRUKTURZE LAMELARNEJ

Micromechanical model of polycrystalline materials with lamellar substructure is presented. The lamellar microstructure of grains is accounted for using the well-established framework developed for layered composites. Within the approach different scale transition rules between the level of lamellar grain and the polycrystalline sample can be employed. The model capabilities are tested using the example of $\alpha 2 + \gamma$-TiAl intermetallic. Elastic properties and the initial yield surface for the lamellar grain (PST crystal) and for the untextured polycrystal are estimated. Elastic and plastic anisotropy degree is analyzed.
Keywords: micromechanics, homogenization, lamellar substructure, anisotropic material, anisotropy degree

Zaprezentowano model mikromechaniczny materiałów polikrystalicznych o substrukturze lamelarnej. Substruktura laminatu obserwowana dla pojedynczego ziarna została uwzględniona przy wykorzystaniu tradycyjnego podejścia przyjmowanego w przypadku kompozytów warstwowych. W ramach proponowanego podejścia stosowane być mogą różne schematy przejścia mikro-makro z poziomu ziarna o substrukturze laminatu do poziomu polikryształu. Możliwości modelu zostały przetestowane na przykładzie intermetaliku $\alpha_2 + \gamma$-TiAl. Wyznaczono własności sprężyste i początkową powierzchnię płynięcia pojedynczego kryształu o substrukturze lamelarnej i polikryształu bez tekstury. Przeanalizowano stopień anizotropii własności sprężystych i plastycznych.

1. Introduction

The paper deals with the polycrystalline materials in which one can distinguish three levels of microstructure (Fig. 1), namely:
(1) Level of an individual lamella;
(2) Level of a lamellar grain, which will be called a *metagrain*, build of colonies of thin parallel plates;
(3) Level of polycrystalline material.
For proper separation of these three levels of microstructure [20], enabling one the formulation of a three-scale micromechanical model, it is required that the thickness of an individual lamella is considerably smaller than the average size of a metagrain, which itself is much smaller than the characteristic dimension of a polycrystalline sample.

As concerns plastic properties of the materials with lamellar substructure, it is observed that the small thickness of the lamellae induces confinement effects (the Hall-Petch effects) by reducing the distance of a main free path for dislocations [1]. These effects are usually taken into account by a morphological differentiation of the plastic deformation modes such as slip or twinning.

Identifying a slip/twin system by $\{\mathbf{m}^r, \mathbf{n}^r\}$, where the unit vector $\mathbf{m}^r$ is coaxial with the direction of shearing and $\mathbf{n}^r$ is a unit normal to the shearing plane for the mode, one defines [17]:

- *longitudinal* modes for which plane and direction of shearing are parallel to the lamellae interface specified by a unit normal $\mathbf{n}$,

* INSTITUTE OF FUNDAMENTAL TECHNOLOGICAL RESEARCH OF POLISH ACADEMY OF SCIENCES, 02-106 WARSZAWA, 5B PAWINSKIEGO STR., POLAND

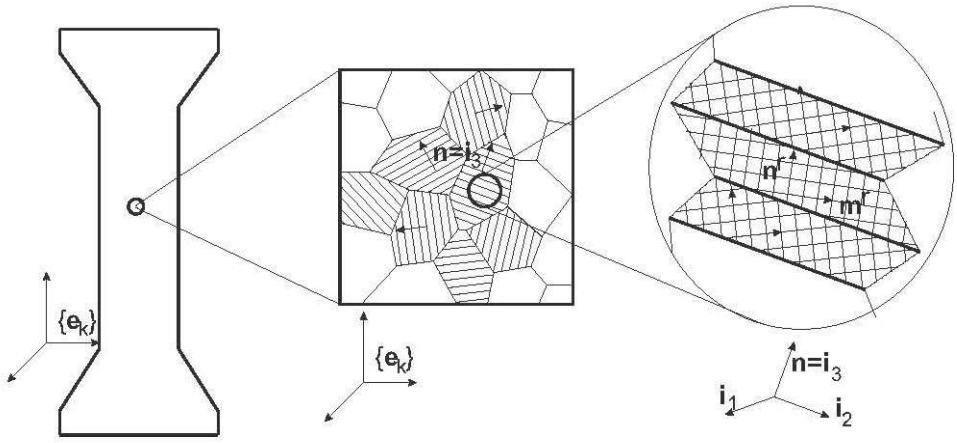

Fig. 1. Polycrystal with lamellar substructure

$$\mathbf{n}^r_{LONG} \cdot \mathbf{n} = 1, \qquad \mathbf{m}^r_{LONG} \cdot \mathbf{n} = 0, \tag{1}$$

- *mixed* modes for which only the direction of shearing is parallel to the lamellae interface,

$$\mathbf{n}^r_{MIX} \cdot \mathbf{n} \neq 1, \qquad \mathbf{m}^r_{MIX} \cdot \mathbf{n} = 0, \tag{2}$$

- *transversal* modes for which neither plane or direction of shearing are parallel to the lamellae interface

$$\mathbf{n}^r_{TRANS} \cdot \mathbf{n} \neq 1, \qquad \mathbf{m}^r_{TRANS} \cdot \mathbf{n} \neq 0, \tag{3}$$

If the deformation mode under consideration belongs to the same type, that is in the case of single crystal one should expect an equal initial critical shear stress τ^r_c, then in the case of lamellar grain one has

$$\begin{aligned} &\tau_c^{TRANS} = \alpha_T \tau_c^{MIX} = \alpha_T \alpha_M \tau_c^{LONG}, \\ &\text{where} \qquad \alpha_T \geqslant 1, \quad \alpha_M \geqslant 1. \end{aligned} \tag{4}$$

and $\tau_c^{LONG} = \tau_c^r$. As it will be demonstrated, these directional confinement effects result in substantial inelastic anisotropy of a metagrain.

Lamellar substructure of grains usually develops due to particular condition during processing. In metals and alloys of high specific strength the lamellar substructure is created as a result of deformation twinning or due to the thermal treatment, e.g. in $\alpha_2 + \gamma$-TiAl intermetallic. This kind of microstructure can be also observed in shape memory alloys and polymers or man-made laminated composites. Consequently, the micromechanical model presented in this paper shares common concepts with the corresponding modelling frameworks formulated for shape memory alloys (SMA) [31], semicrystalline polymers [21] or composites [5, 2]. In most of these models attention is focused on the linear elasticity or linear elasticity with the eigenstrain (transformation strain in the case of SMA). The idea of a three-scale model has been also utilized in the family of models developed in order to relax the strong constraints imposed on the deformation by the Taylor scheme in the case of crystal plasticity (the so-called pancake model [10, 36], LAMEL model or ALAMEL model, [37, 38]). The similar concept has been recently applied in modelling of the polycrystalline SMA [31].

In the next section the attention is focused on the scale transition rule between level 1 and level 2. We present an approach for modelling of a lamellar microstructure within a small strain regime, assuming that material is described by linear or non-linear constitutive laws. The general framework developed for laminates (layered composites) is used, cf. e.g. [5]. The three scale models, which employ different transition schemes between the level of lamellar grain and the level of polycrystal are then presented. In section 3 we apply the proposed approach to study elastic and plastic anisotropy of the two-phase $\alpha_2 + \gamma$-TiAl intermetallic of lamellar substructure. It is analyzed how the predicted overall properties vary with the metagrain geometry and scale transition rules applied. Extended description of the presented modelling framework and discussion on results can be found in [14]. Additionally, in the present paper the intensity of anisotropy of elastic properties at the local level and at the intermediate level is quantified. It is demonstrated that, contrary to inelastic anisotropy, the lamellar substructure of the metagrain lowers its overall elastic anisotropy as compared to the anisotropy of constituent phases. 3-scale micromechanical model of TiAl polycrystals was also formulated in [25]. In this paper, contrary to [25], we analyze the influence of modelling scheme on the predicted overall properties.

Throughout the work, the following notation for tensor operations is used. Let $\mathbf{v}$, $\mathbf{u}$,v_i, u_i denote vectors and

their representation in some orthonormal basis, $\mathbf{T}$, T_{ij} – a second order tensor and its representation and $\mathbb{A}, \mathbb{B}$, A_{ijkl}, B_{ijkl} – fourth order tensors and their representations then

$$\mathbf{v} \otimes \mathbf{u} \leftrightarrow v_i u_j,\ \mathbf{T} \cdot \mathbf{v} \leftrightarrow A_{ij} v_j,\ \mathbb{A} \cdot \mathbf{T} \leftrightarrow A_{ijkl} T_{kl},$$
$$\mathbb{A} \circ \mathbb{B} \leftrightarrow A_{ijkl} B_{klmn}\ .$$

2. Scale transition rules

2.1. The model of the metagrain

The analysis is restricted to the small strains and rotations. Following the approach developed for the layered composites (e.g. [5]), at the interface of normal $\mathbf{n}$ between neighboring lamellae i and j a standard condition of continuity of displacement (or velocity) field is fulfilled implying the following compatibility condition for small strain (or strain-rate) tensor

$$\boldsymbol{\varepsilon}_j = \boldsymbol{\varepsilon}_i + \frac{1}{2}\left(\mathbf{b} \otimes \mathbf{n} + \mathbf{n} \otimes \mathbf{b}\right), \tag{5}$$

where $\mathbf{b}$ is an arbitrary vector. Furthermore, assumption of equilibrium of traction forces at this interface implies for the local stress tensor

$$\boldsymbol{\sigma}_j \cdot \mathbf{n} = \boldsymbol{\sigma}_i \cdot \mathbf{n}. \tag{6}$$

It is also assumed that the stress and strain fields are uniform within the lamella. As a result of the above conditions, the components of the strain and stress tensors in the lamellae i and j are related as follows (see Fig. 1)

$$\begin{aligned} &\mathbb{P}^L \cdot \boldsymbol{\varepsilon}_i = \mathbb{P}^L \cdot \boldsymbol{\varepsilon}_j = \mathbb{P}^L \cdot \boldsymbol{\varepsilon}_{mc}, \\ &\mathbb{P}^T \cdot \boldsymbol{\sigma}_i = \mathbb{P}^T \cdot \boldsymbol{\sigma}_j = \mathbb{P}^T \cdot \boldsymbol{\sigma}_{mc}, \end{aligned} \tag{7}$$

where ε_{mc} and σ_{mc} are average strain and stress tensors in the metagrain defined as

$$\boldsymbol{\varepsilon}_{mc} = \{\boldsymbol{\varepsilon}_i\}, \quad \boldsymbol{\sigma}_{mc} = \{\boldsymbol{\sigma}_i\}, \quad \{\cdot\} = \sum_{i=1}^{NL} v_i \, (\cdot)_i \tag{8}$$

and NL is the number of distinct lamellae in the metagrain; $v_i = V_i/V_{mc}$ are their relative volume contents. The fourth order tensors $\mathbb{P}^T$ and $\mathbb{P}^L$ are two orthogonal projectors specified by formulae [39, 24]:

$$\begin{aligned} &\left(\mathbb{P}^T\right)_{ijkl} = \tfrac{1}{4}\left(2\delta_{ik} n_j n_i + \delta_{jk} n_j n_i + \delta_{il} n_j n_k\right), \\ &\mathbb{P}^L = \mathbb{I}^S - \mathbb{P}^T, \end{aligned} \tag{9}$$

which project second order tensors into two three-dimensional orthogonal sub-spaces ($\mathbb{I}^S$ is the fourth order symmetrized identity tensor).

It is assumed that the constitutive law between a strain (or a strain-rate) measure and a stress measure in the lamella i is linear (or that it can be linearized) with the corresponding compliance tensor $\mathbb{M}_i$ and the eigen-strain (the reference strain) ε_i^{res}, namely

$$\boldsymbol{\varepsilon}_{\mathrm{i}} = \mathbb{M}_i \cdot \boldsymbol{\sigma}_i + \boldsymbol{\varepsilon}_i^{\mathrm{res}}, \quad \boldsymbol{\sigma}_i = \mathbb{L}_i \cdot \left(\boldsymbol{\varepsilon}_i - \boldsymbol{\varepsilon}_i^{\mathrm{res}}\right), \quad \mathbb{L}_i = \mathbb{M}_i^{-1}. \tag{10}$$

We are looking for the homogenized properties $\mathbb{M}_{mc}$ of a laminated metagrain and the overall eigen-strain (the overall reference strain) in the metagrain $\boldsymbol{\varepsilon}_{mc}^{res}$ which relate the average strain $\boldsymbol{\varepsilon}_{mc}$ and the stress $\boldsymbol{\sigma}_{mc}$ according to the following relation

$$\begin{aligned} &\boldsymbol{\varepsilon}_{\mathrm{mc}} = \mathbb{M}_{mc} \cdot \boldsymbol{\sigma}_{mc} + \boldsymbol{\varepsilon}_{mc}^{\mathrm{res}}, \quad \boldsymbol{\sigma}_{mc} = \mathbb{L}_{mc} \cdot \left(\boldsymbol{\varepsilon}_{mc} - \boldsymbol{\varepsilon}_{mc}^{\mathrm{res}}\right), \\ &\mathbb{L}_{mc} = \mathbb{M}_{mc}^{-1}. \end{aligned} \tag{11}$$

To this end we follow to some extent the derivations presented in [5, 31] which relay on the decomposition of the second-order tensor into out-of-plane and in-plane parts. This decomposition is realized by the orthogonal projectors (2.9).

Using Eqs(2.7)-(2.11) the overall compliance tensor of a metagrain $\mathbb{M}_{mc}$ and the overall eigen-strain $\varepsilon_{mc}^{\mathrm{res}}$ are found. Localization tensor $\mathbb{A}_i$ and concentration tensor $\mathbb{B}_i$ defined as

$$\boldsymbol{\varepsilon}_i = \mathbb{A}_i \cdot \boldsymbol{\varepsilon}_{mc} + \alpha_i, \quad \boldsymbol{\sigma}_i = \mathbb{B}_i \cdot \boldsymbol{\sigma}_{mc} + \beta_i \tag{12}$$

can be also obtained. The corresponding relations are collected in the Appendix A.

Note that computation of the homogenized properties of a metagrain is not necessary if our only task is to find local stresses and strains in lamellae under imposed average strain ε_{mc} (or stress $\boldsymbol{\sigma}_{mc}$) in the metagrain. Eqs. (2.7), the definitions (2.8) and the local constitutive relations (2.10) constitute the set of $6NL$ +3 equations sufficient to find $6NL$ +3 independent components of unknowns: $\boldsymbol{\varepsilon}_i^T$, $\boldsymbol{\sigma}_i^L$, $\boldsymbol{\sigma}_{mc}$ (or ε_{mc}). The latter observation is also true if the constitutive relation is non-linear (e.g. the viscoplastic power-law). In the latter case the obtained equations are non-linear and they are solved e.g using the Newton-Raphson (N-R) method. The specification of the homogenized properties of a metagrain is necessary when we have to do with three-scale (or, in general, multi-scale) modelling. In such a case compliances $\mathbb{M}_{mc}$ serve as local properties in the transition scheme between the level of a metagrain and the level of a polycrystalline sample. Computational issues related to the 3-scale modelling will be discussed below.

2.2. The model of the polycrystal

In order to obtain the overall response of polycrystalline material of lamellar substructure three different scale transition rules between the level of a metagrain and the level of a polycrystalline sample have been considered:

(1) **The Voigt (Taylor) model (upper bound).** The relations between the overall stress $\mathbf{\Sigma}$ and the overall strain $\mathbf{E}$ (or the strain-rate $\dot{\mathbf{E}}$) and the corresponding average quantities in the metagrain are

$$\mathbf{E} = \boldsymbol{\varepsilon}_{mc}, \qquad \sum = \langle \boldsymbol{\sigma}_{mc} \rangle = \sum_{mc=1}^{NG} v_{mc} \boldsymbol{\sigma}_{mc}, \tag{13}$$

where NG is the number of metagrains in the polycrystalline aggregate.

(2) **The Reuss (Sachs) model (lower bound).** The relations between the overall stress $\mathbf{\Sigma}$ and the overall strain $\mathbf{E}$ (or the strain-rate $\dot{\mathbf{E}}$) and the corresponding average quantities in the metagrain are

$$\boldsymbol{\sigma} = \boldsymbol{\sigma}_{mc}, \quad \mathbf{E} = \langle \boldsymbol{\varepsilon}_{mc} \rangle = \sum_{mc=1}^{NG} v_{mc} \boldsymbol{\varepsilon}_{mc}. \tag{14}$$

(3) **The self-consistent model.** This estimation of an overall behaviour of polycrystal relays on Eshelby's solution [6] for the ellipsoidal inclusion embedded in the infinite medium. In the frame of the self-consistent model a single grain is considered as an inclusion while the medium has averaged, yet unknown, properties of a polycrystal. According to this model the relations between the overall stress $\mathbf{\Sigma}$ and the overall strain $\mathbf{E}$ (or the strain-rate $\mathbf{D} = \dot{\mathbf{E}}$) and the corresponding average quantities in the metagrain are [7, 43]

$$\begin{aligned} &\boldsymbol{\varepsilon}_{mc} - \mathbf{E} = -\mathbb{M}_*^{SC} \cdot (\boldsymbol{\sigma}_{mc} - \sum), \quad \sum = \langle \boldsymbol{\sigma}_{mc} \rangle, \\ &\mathbf{E} = \langle \boldsymbol{\varepsilon}_{mc} \rangle \end{aligned} \tag{15}$$

where the fourth order tensor $\mathbb{M}_*^{SC}$ is the inverse of the so-called Hill's tensor which depends on the inclusion shape and the properties of the equivalent medium specified by $\mathbb{L}$. In the example analyzed below a spherical shape of metagrains is assumed.

Using the above models one can find the overall properties and the overall response of a polycrystal governed by the linear (or linearized) relation

$$\mathbf{E} = \bar{\mathbb{M}} \cdot \sum + \mathbf{E}^{res} \quad \sum = \bar{\mathbb{L}} \cdot (\mathbf{E} - \mathbf{E}^{res}), \quad \bar{\mathbb{L}} = \bar{\mathbb{M}}^{-1}. \tag{16}$$

3. Application to $\alpha_2 + \gamma$-TiAl of lamellar substructure

3.1. Description of microstructure

The microstructure of polysynthetically-twinned (PST) $\alpha_2 + \gamma$-TiAl has been described in detail in [1] or [40, 41], therefore we will only recapitulate basic facts. In this two phase material a strict orientation relationship exists between the hexagonal α_2 phase and the fcc-like γ phase of tetragonal symmetry, namely the closely packed planes, (0001) in α_2 and {111} in γ, and crystallographic directions $\langle 1\bar{1}0 \rangle$ in γ and $\langle 11\bar{2}0 \rangle$ in α_2 are parallel. This relationship is fulfilled by six distinct orientation variants of γ-phase corresponding to three twin-related pairs, Fig. 2.

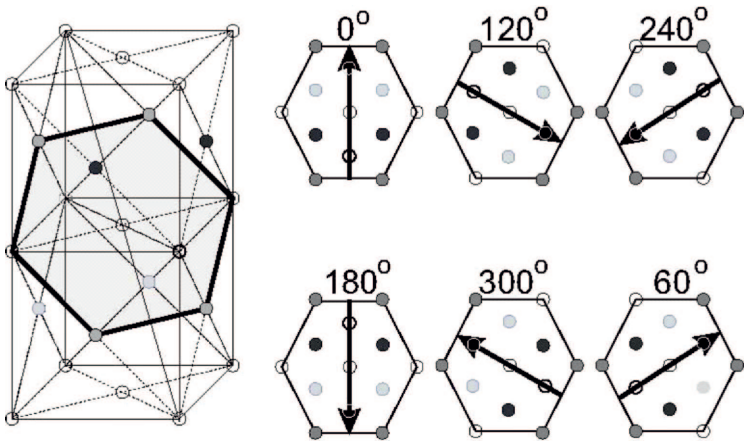

Fig. 2. Orientation variants of γ phase in PST $\alpha_2 + \gamma$ TiAl crystal (see also [41]); filled circles denote Al atoms

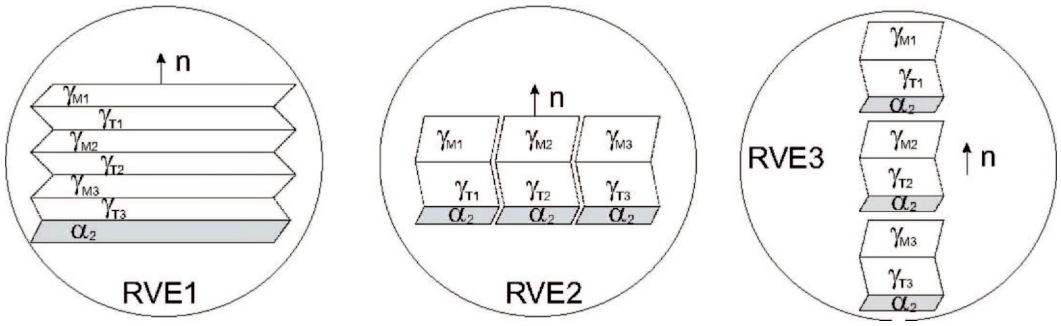

Fig. 3. Considered types of RVE for the metagrain

Let us study mechanical properties of a metagrain made of this material. We start with the elastic anisotropy and then turn to inelastic properties. Three types of a laminated unit cell (RVE) for the derivation of the overall properties of a metagrain are considered. They are presented in Fig 3. In the case of RVE1 a laminate is composed of 7 distinct lamellae. In the case of RVE2 and RVE3 the laminated component of RVE is composed of 3 distinct lamellae: one α_2 lamella and two γ lamellae being one of the three twin-related pairs, Fig. 2. Subsequently, the overall properties of the metagrain are obtained assuming equal strain or equal stress in each of three possible sub-laminates, correspondingly. Additionally, the upper (RVEV) and lower (RVER) bounds are derived. They are obtained assuming equal strain or equal stress in each of seven lamellae.

In further derivations we assume that six admissible variants of γ lamellae have equal volume fractions, therefore we have for a laminate of RVE1

$$v_i = \frac{1}{6}(1 - v_\alpha) \quad \text{for} \quad i = 1, ..., 6, \quad v_7 = v_\alpha \qquad (17)$$

and for an individual laminated component of RVE2 and RVE3

$$v_i = \frac{1}{2}(1 - v_\alpha) \quad \text{for} \quad i = 1, 2, \quad (k = 1, 3, 5), \quad v_3 = v_\alpha \qquad (18)$$

The overall properties of a metagrain depend on the volume fraction v_α of phase α_2.

3.2. Elastic properties

In the micromechanical modelling, in spite of the geometry of microstructure, in order to estimate the overall properties one has to know the local ones. The independent components of the local elasticity tensors $\mathbb{L}_i^e$ of the single crystals of γ-TiAl and α_2-Ti_3Al phases are collected in Table 1. In view of the lattice symmetry the elasticity tensor for γ phase has tetragonal symmetry while for α_2 phase is transversely isotropic. As it can be verified performing the spectral decomposition of $\mathbb{L}_i$ [28] and using the anisotropy measures introduced in the Appendix B, the local elastic anisotropy is not strong.

TABLE 1
Independent components of local elasticity tensors [GPa] in the phases [34, 35]

Phase	L_{2222}	L_{2233}	L_{1122}	L_{1111}	L_{1212}	L_{3232}
α_2-Ti_3Al	175	88.7	62.3	220	62.6	
γ-TiAl	183	74.1	74.4	178	105	78.4

TABLE 2
Spectral decompositions of local elasticity tensors in the phases, h_K – Kelvin modulae [GPa], $\Phi(\eta) = \arctan[\mathrm{sgn}(\eta)3(\sqrt{2}|\eta|)^{1/3}]$, η – stiffness distributor (for the details see [16])

Phase	h_{VI}	h_V	h_{IV}	h_{III}	$h_{II} = h_I$	$\Phi[^\circ]$	ζ	η
α_2-Ti_3Al	332.6	151.1	86.4		125.2	2.77	0.56	0.017
γ-TiAl	330.0	105.1	108.9	156.8	210	-0.56	0.69	0.023

Independently of v_α and the assumed type of RVE the overall elasticity tensor $\mathbb{L}_{mc}^e$ of a metagrain is transversely isotropic (although, the laminated subcomponent for RVE2 and RVE3 is not). The main axis of symmetry is coaxial with the unit normal **n** to the lamellae interfaces. Fig. 4 presents the variation of four distinct Kelvin moduli with the volume fraction of α_2 phase calculated for all considered types of RVE. As it is seen differences between results obtained for three RVEs depicted in Fig. 3 are almost negligible. Similarly, the upper and lower bounds are quite close to each other except of the modulus h_3^{mc} for which they are relatively far from each other. As far as dependence of metagrain moduli on the volume fraction of α_2 phase is concerned, it has a significant impact on moduli h_2^{mc} and h_3^{mc} while moduli h_1^{mc} and h_4^{mc} almost do not vary with v_α. The value of angle $\Phi(\eta^{mc})$ varies insignificantly with the RVE model. It monotonically increases with v_α from around 0.1° to

2.8°, so it remains very small. Consequently, the metagrain of this two-phase material is almost volumetrically isotropic justifying the use ζ-measure of anisotropy (B.1).

Note that for transversely isotropic material [12, 16]:

- The Kelvin moduli $h_3^{mc} = h_{III} = h_{IV}$ and $h_4^{mc} = h_I = h_{II}$ are two distinct shear moduli valid for shear deformations in the plane perpendicular to **n** and in the planes coaxial with **n**, respectively.
- The Kelvin moduli $h_1^{mc} = h_{VI}$ and $h_2^{mc} = h_V$ are the moduli valid for two deformations (eigen-states) being the combinations of the hydrostatic state and the deviatoric deformation specified by $\boldsymbol{\varepsilon} = \varepsilon(3\mathbf{n} \otimes \mathbf{n} - \mathbf{I})$. The way by which these two states are combined for the considered material is specified by the stiffness distributor η^{mc}. If η^{mc}=0 then h_1^{mc} is the bulk modulus while h_2^{mc} is deviatoric modulus for $\boldsymbol{\varepsilon} = \varepsilon(3\mathbf{n} \otimes \mathbf{n} - \mathbf{I})$. In the latter case material is volumetrically isotropic.

The measures of anisotropy of the derived $\mathbb{L}_{mc}^{e}$ as a functions of v_α are presented in Fig. 5. Since the differences between $\mathbb{L}_{mc}^{e}$ obtained for RVE1, RVE2 and RVE3 have been almost negligible, only the intensities of anisotropy for RVE1, the upper bound (UP (RVEV)) and lower bound (LO (RVER)) models of the metagrain are compared. It is seen that the presence of six orientation variants of γ phase within the metagrain decreases the anisotropy factors as compare to single γ lamella or α_2 lamella (see Table 2). The value of α_2 content corresponding to the minimum values of anisotropy factors are collected in Table 3.

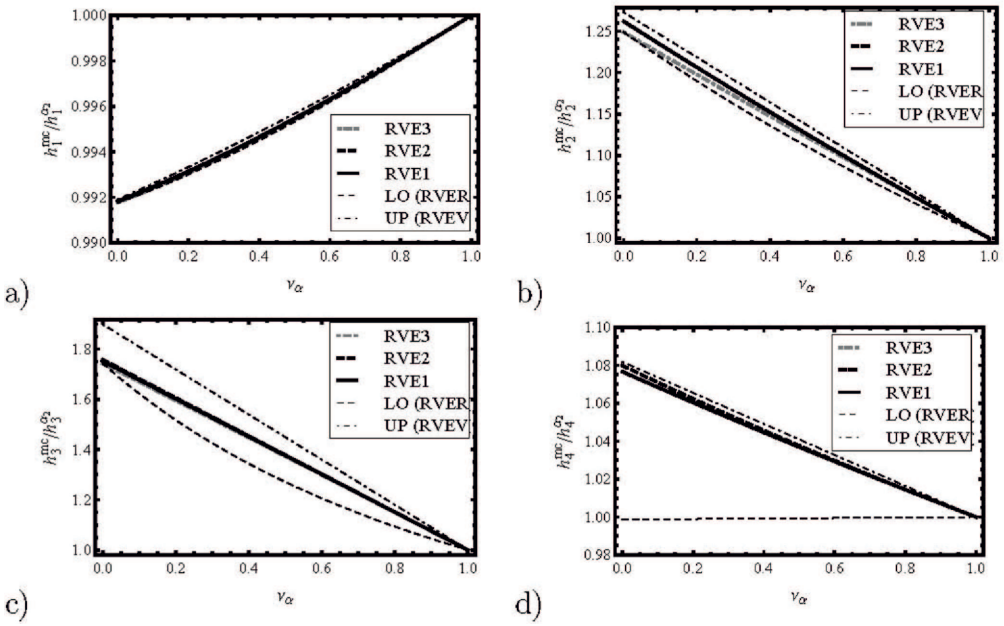

Fig. 4. The calculated elastic Kelvin moduli of a metagrain obtained for different models of RVE. Because α_2-phase is also transversely isotropic, the Kelvin moduli h_i^{mc} are scaled by the corresponding moduli $h_i^{\alpha_2}$ (see Table 1)

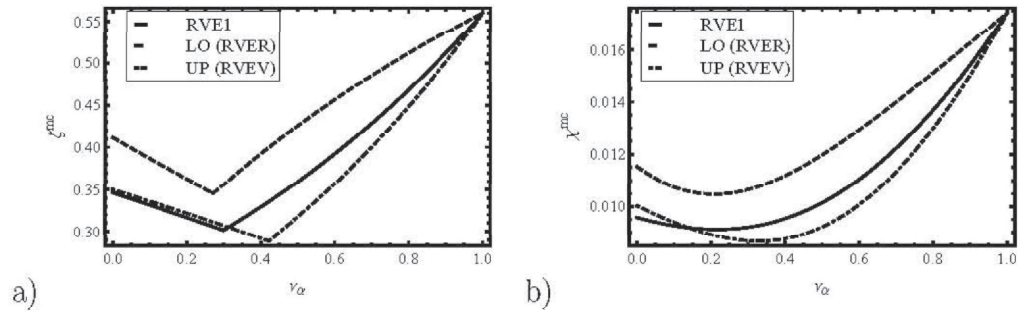

Fig. 5. Intensity of elastic anisotropy of a metagrain obtained for different models of RVE

TABLE 3
The volume content of α_2 phase in the metagrain for which the corresponding measure of anisotropy takes the minimum value

	RVE1	RVER	RVEV
ζ^{mc}	0.300	0.272	0.422
χ^{mc}	0.217	0.208	0.329

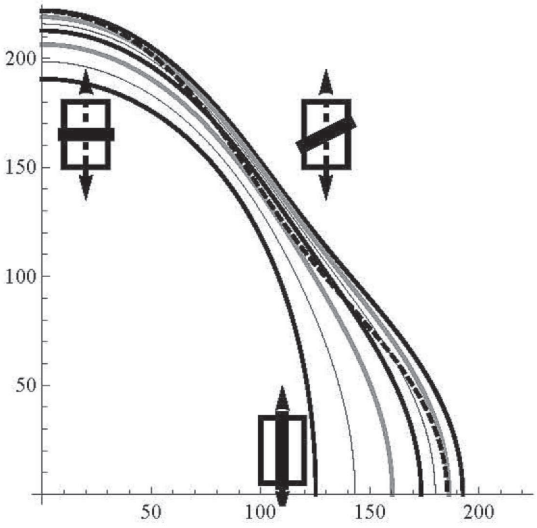

Fig. 6. Dependence of the directional Young modulus [GPa] for PST $\alpha_2 + \gamma$-TiAl (a single metagrain) on the volume fraction of α_2 phase. The outer line corresponds to ν_α =0 while the inner line to ν_α =1. In between lines are for ν_α = {0.1, 0.2, 0.3, 0.5, 0.75}. The dashed curve corresponds to the measured elasticity tensor of PST TiAl [23]

The anisotropy of the metagrain can be also study with use of the directional Young modulus [22]

$$E^{mc}(\mathbf{m}) = ((\mathbf{m} \otimes \mathbf{m}) \cdot \mathbb{M}^e_{mc} \cdot (\mathbf{m} \otimes \mathbf{m}))^{-1}, \qquad (19)$$

where $\mathbf{m}$ is any unit vector[1)]. Fig. 6 presents the directional Young modulus of PST $\alpha_2 + \gamma$-TiAl in the case of the metagrain represented by RVE1 for different values of ν_α in the form of polar plot. Generally, with the increasing volume fraction of α_2 phase the Young modulus decreases for any direction. Moreover, the volume fraction of α_2 phase has the most significant impact on the Young modulus in the directions coaxial with the laminate interface. For experimentally observed values of $\nu_\alpha \cong 01$ one obtains the relation

$$E^{mc}(0^\circ) > E^{mc}(90^\circ) > E^{mc}(\phi^*), \quad \phi^* \in (30^\circ, 60^\circ), \quad (20)$$

where $\cos\phi = \mathbf{m}\cdot\mathbf{n}$. Such relation is qualitatively confirmed by experiments [9]. The independent components of the elasticity tensor of PST crystal of TiAl has been measured by Tanaka (see [23] for the respective values). The directional Young modulus corresponding to the measured $\mathbb{L}^e_{mc}$ is marked in Fig. 6 by a dashed line. In general, it lies within the theoretically predicted values for relatively small content of α_2 phase (not clearly reported in [23]). The most significant difference is obtained for intermediate directions. In [42] the Young modulus E = 175 GPa for the polycrystalline TiAl of lamellar microstructure has been measured. The extrusion texture of a tested sample indicates the case for which the direction $\mathbf{n}$ is close to be perpendicular to the tension direction. As it is seen in Fig. 6 the experimentally obtained value is reproduced quite well for the reasonable content of α_2 phase (again, not clearly reported in [42]).

Finally, using the results of spectral decomposition for the stiffness tensor of the metagrain the bound and the self-consistent estimates of overall elastic properties of untextured polycrystal composed of metagrains are evaluated according to the procedure formulated in [13]. In Fig. 7 the comparison of the overall Young modulus and the overall shear modulus obtained with use of different scale transition rules between the level of metagrain and the level of polycrystalline sample (see Section 2.2) are presented as functions of ν_α. Different RVEs denote different models of a metagrain, that is different scale transition rule employed between the level 1 and the level 2. It is seen that for RVE1 the bounds are very tight and the SC estimator almost coincide with the Hill estimate defined as an average of the upper and lower bound. The same behaviour is observed for two remaining RVEs presented in Fig. 3. For a low content of α_2 phase the scale transition rule between level 1 and 2 influences more on the predicted overall property than the scale transition rule between level 2 and level 3. This trend is reversed for a high content of α_2 phase, as expected. In the figures the self-consistent estimates of $\bar{E}$ and $\bar{G}$ obtained for the two-phase material without introduction of an additional level of microstructure (denoted as "2 scale (SC)") are also presented. When calculating the latter estimates the orientation relationships between α_2 and γ lamellae are not taken into account. Differences between self-consistent estimates obtained for 3-scale and 2-scale microstructure are not substantial. They are the strongest for comparable contents of both phases.

[1)] In analogy with the meaning of Young's modulus for isotropic materials, $E(\mathbf{m})$ is the slop of curve presenting the dependence of the stress on the strain component in the loading direction in uniaxial tension or compression along $\mathbf{m}$ direction

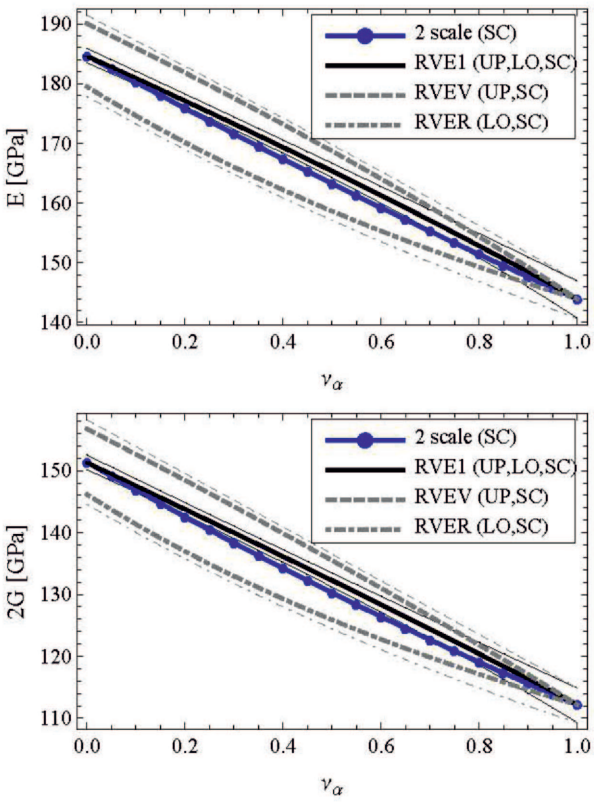

Fig. 7. Bounds (UP,LO) and self-consistent (SC) estimates of the overall Young modulus and the overall shear modulus for random polycrystal of two-phase TiAl with lamellar substructure and different models of the metagrain

3.3. Initial yield surface

Now, let us pass to the inelastic properties of TiAl of lamellar substructure. First, we will study the anisotropy of an *initial* yield stress of a metagrain induced mainly by the confinement effects discussed in the introduction. We will consider the so-called micro-yielding. To this end we identify *initiation of yielding of a metagrain with initiation of slip or twinning on any of possible systems in any of lamellae*. According to the above definition initiation of yielding of a PST metagrain is equivalent to the limit of elasticity in one of the lamellae and must be established with use of a local stress. Consequently, this local stress in the lamellae, under the prescribed overall stress $\boldsymbol{\sigma}_{mc}$, is obtained employing the concentration equations (2.12), where tensors $\mathbb{B}_i$ are calculated with use of the elastic compliances and $\boldsymbol{\beta}_\mathbf{i}= \mathbf{0}$. Initiation of slip or twinning within lamellae is governed by the extended Schmid law formulated in [33]. In the examples shown below the PST metagrain is modelled by RVE1.

γ-TiAl has fcc like structure. Due to the space distribution of Ti and Al atoms, slip systems relevant for fcc materials are subdivided into two groups [1]: 4 ordinary dislocations $\{111\}\langle 10\bar{1}]$ and 8 super dislocations $\{111\}\langle 1\bar{1}0]$. It is observed in experiments [1] that super-dislocations are more difficult to initiate than ordinary dislocations. Note that, there are only 3 ordinary dislocations which are independent while there are 5 independent slip systems within super-dislocation group. There are only 4 twin systems: $\{111\}\langle 11\bar{2}]$. As concerns α_2 phase, three types of slip systems are usually invoked: basal $(0001)\langle 11\bar{2}0\rangle$, prismatic $\{1\bar{1}00\}\langle 11\bar{2}0\rangle$ and pyramidal $(2c + a)\{11\bar{2}1\}\langle\bar{1}\bar{1}26\rangle$. As reported in the literature [10, 11, 25] the prismatic slip systems are most easily initiated, while remaining two groups are difficult to initiate. One should note that the easy prismatic mode, in view of its orientation with respect to the lamellae interface, is the mixed mode, therefore initiation of the plastic yielding within α_2 lamellae requires much higher level of stress than in γ lamellae. The performed study indicates that the hard modes in γ and α_2 phases have no influence on the value of the initial yield stress defined as above, thus in further analysis the hard modes (super-dislocations in γ phase and two hard modes in α_2 phase) have been neglected. Furthermore, following [25], we have assumed

$$\tau_c^{prism} = 2\tau_c^{ord}. \tag{21}$$

The value of critical shear stress for twinning mode in single crystal of γ-TiAl is usually close to the value of τ_c^{ord}. If not indicated explicitly, in calculations $\rho^{twin} = \tau_c^{twin}/\tau_c^{ord} = 1.1$ has been assumed.

In Fig. 8 an identification procedure for confinement parameters α_M and α_T defined by (1.4), is illustrated. As it is shown without the morphological differentiation of the plastic deformation modes ($\alpha_M = \alpha_T = 1$) one is not able to reproduce the strong anisotropy of the uniaxial yield stress of PST metagrain observed in the experiments. The experimental data for tension at room temperature of PST in five different directions with respect to **n** has been taken from [1]. They concern two-phase PST γ-Ti49Al-alloys without ternary alloying additions (see page 195, Fig. 8 in [1]). It can be verified that α_T, defined by (1.4), does not influence on the initial yield stress in the direction perpendicular to **n**, therefore first, value of α_M is established (see Fig. 8(a)), and then α_T (see Fig. 8(b)). The value of the yield stress for the intermediate direction specified by $\phi = 40^\circ$ is independent of both confinement parameters, therefore it has been used as a reference value, where the measured value of σy $(40^\circ) \simeq$ 100 MPa. As a result of this identification procedure one finds: α_M =2.8, α_T =1.25 and τ_c^{ord}= 50 [MPa]. Similar values have been established in [17]; however, for a flow stress defined with use of the viscoplastic power law. In Fig. 9 the directional yield stress in compression is presented and compared with the experimental data found in [40]. Details concerning the experiment condition and

material composition were not provided in the reference, nevertheless the agreement with the values obtained with use of identified parameters is quite good. In Fig. 9 the shape of the cross-section of the initial yield surface for the bi-axial stress state is shown. One observes strong anisotropy of this yield surface.

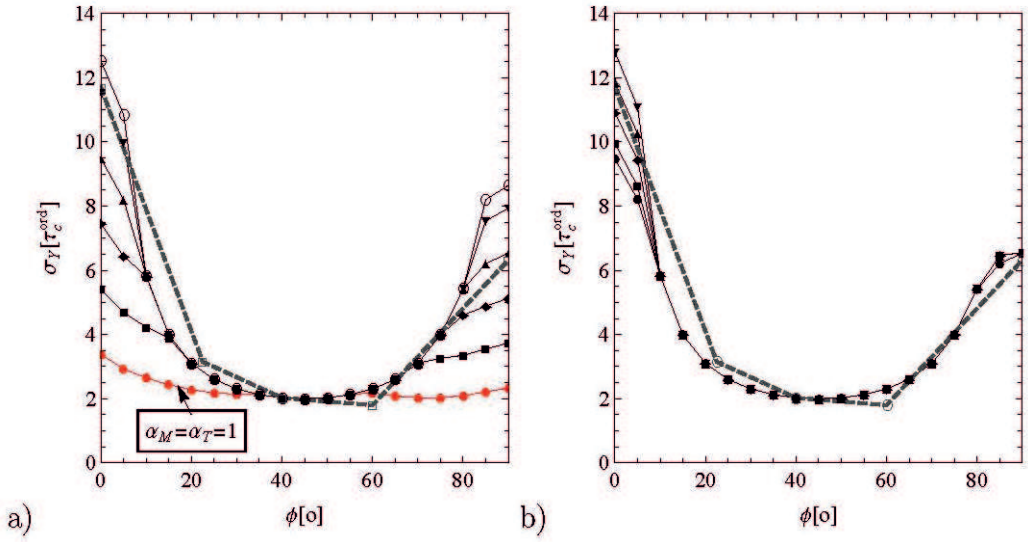

Fig. 8. Illustration of the identification procedure for confinement parameters. The directional initial yield stress in tension (ϕ denotes the angle between unit normal to the interface and the loading direction) for a) different values of α_M = {1.0, 1.9, 2.5, 2.8, 3.4, 4.0},(α_T =1), b) different values of α_T = {1, 1.05, 1.15, 1.25, 1.65} and α_M =2.8; dashed gray line: experimental data [1]

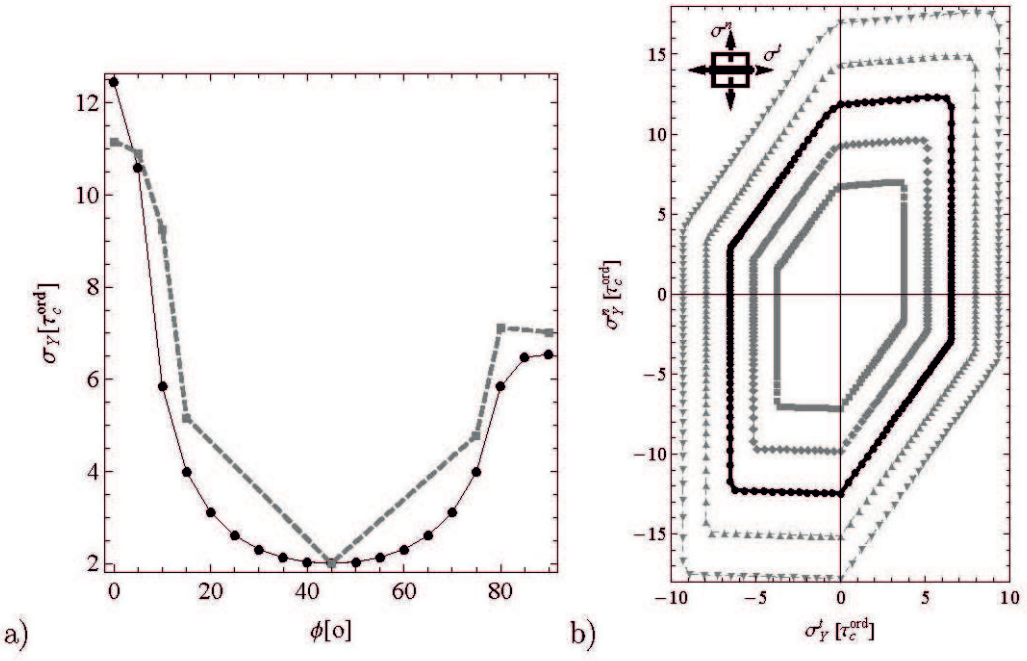

Fig. 9. a) The initial yield stress in compression obtained with use of identified parameters (continuous line) and experimental data [40] (dashed line); b) the initial yield surface for the bi-axial stress state for identified parameters (black line with circles), for different values of α_M = {1.6, 2.2, 3.4, 4.0} (gray lines). Schematic figure presents the orientation of the analysed loading with respect to the lamellae interfaces

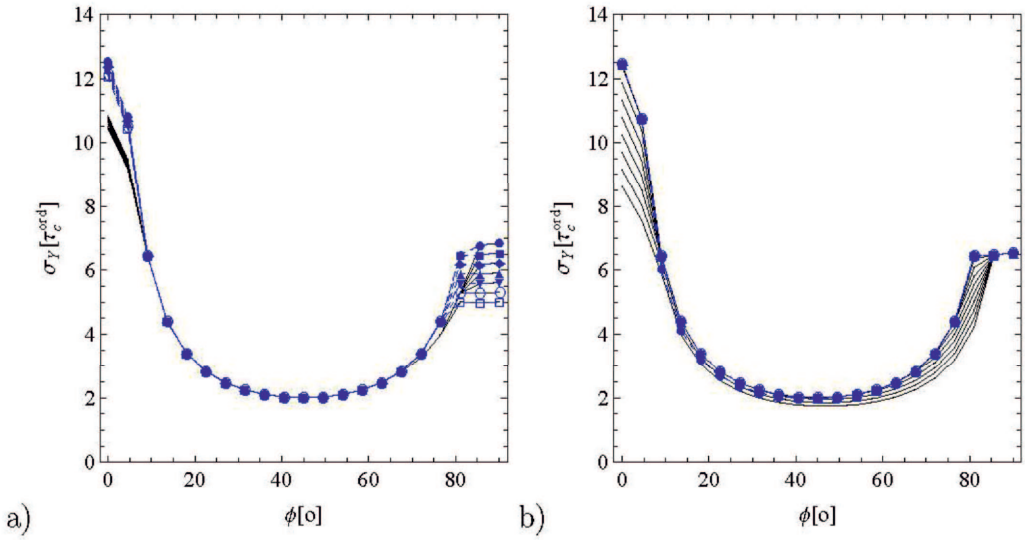

Fig. 10. Initial yield stress in tension (continuous lines) and compression (dashed lines with markers) for a) different values of ν_α, the top curve – ν_α = 0, the bottom curve: ν_α = 0.7, spacing $\Delta\nu_\alpha$ =0.1, ρ^{twin} =1; b) different values of $\rho^{twin} = \tau_c^{twin}/\tau_c^{ord}$, the top curve – ρ^{twin} = 1.2, the bottom curve ρ^{twin} = 0.8, spacing $\Delta\rho^{twin}$ = 0.05, ν_α = 0.1. Confinement parameters: α_T =1.25, α_M =2.8

In Fig. 10(a) the influence of volume fraction of α_2 phase on the directional initial yield stress in tension and compression is demonstrated. It is seen that the volume content of α_2 has the most significant impact on the yield stress when tension/compression direction is coaxial with the interface of lamella. In Fig. 10(b) the effect of ratio ρ^{twin} is studied. In general, twining is the source of a tension-compression asymmetry of a yield stress. In the case of the considered material this asymmetry is the strongest for the direction perpendicular to the lamella interface and the less significant for the intermediate directions. Note also that when τ_c^r for twinning is sufficiently high, then twinning does not influence on the initial yielding.

We close this section with the derivation of the initial yield surface for untextured polycrystal of lamellar substructure. Initiation of plastic yielding is now identified with initiation of yielding in any metagrain, within any of its constituent lamellae on any of slip or twin systems (compare [8, 3]). In Fig. 11 the obtained yield surface is presented for the identified material parameters and ρ^{twin} = 1.1 and ρ^{twin} = 0.7. Performed studies indicated that the tension-compression asymmetry of the initial yield surface of polycrystal will be observed for ρ^{twin} lower than one or close to one, see Fig. 12a. For the experimentally justified value (i.e. ρ^{twin}=1.1) this asymmetry is not present and, similarly as it has been found for fcc untextured polycrystals in [8], the obtained yield surface is the Tresca polyhedron specified by the condition

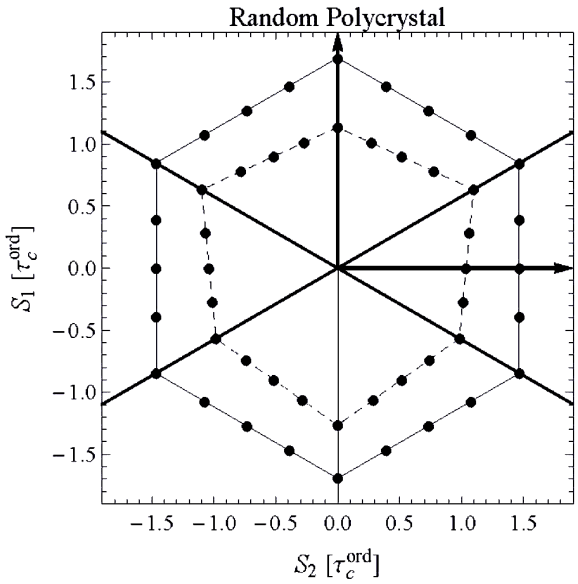

Fig. 11. Initial yield surface for untextured polycrystal of $\alpha_2 + \gamma$-TiAl of lamellar substructure in deviatoric plane (α_T =1.25, α_M =2.8, ν_α =0.1), continuous line ρ^{twin}=1.1, dashed line ρ^{twin} = 0.7; $S_1 = 1/\sqrt{6}(2\Sigma_3 - \Sigma_1 - \Sigma_2)$, $S_2 = 1/\sqrt{2}(\Sigma_1 - \Sigma_2)$

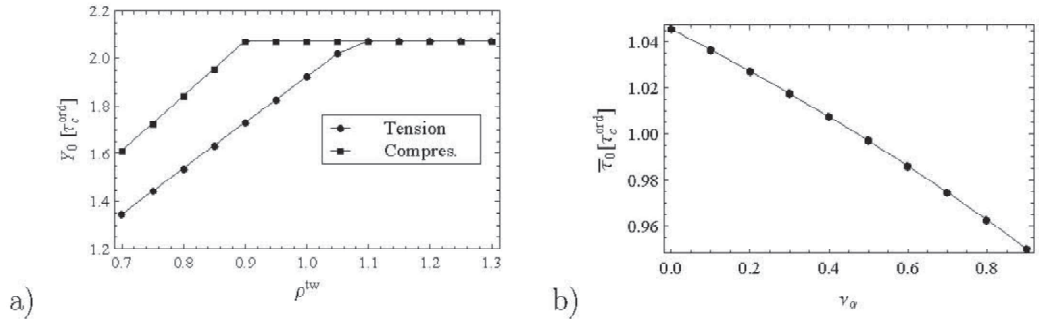

Fig. 12. a)Initial yield stress in uniaxial tension and compression for untextured polycrystal of $\alpha_2 + \gamma$-TiAl of lamellar substructure (α_T = 1.25, α_M=2.8, ν_α= 0.1) as function of ρ^{twin}, b) Initial yield stress in shear (α_T=1.25, α_M =2.8, ν_α=0.1, ρ^{twin}=1.1)as function of ν_α

$$\bar{\tau}_{max} = \bar{\tau}_0, \tag{22}$$

where $\bar{\tau}_{max}$ is the maximum macroscopic shear stress. The size of the yield surface, specified by the parameter $\bar{\tau}_0$, is almost not affected by the confinement parameters. It is governed by the volume fraction of α_2 phase and the value of the critical yield stress on the easiest slip system, see Fig. 12b.

4. Summary

In the paper a three-scale micromechanical approach to estimate overall properties of polycrystalline material of lamellar substructure has been formulated. The way by which the modelling scheme is constructed enables one to employ different scale transition rules between the metagrain level and the level of polycrystalline sample.

The capabilities of the model are thoroughly explored using the example of $\alpha_2 + \gamma$-TiAl intermetallic. The elastic properties and the initial yield surface of the metagrain (i.e. PST crystal) are estimated with the use of different variants of the proposed framework and then compared with the available experimental data. The important part of the performed analysis is the study of the so-called confinement effects invoked by the existence of lamellar substructure. These effects influence on the inelastic deformation resulting in substantial anisotropy of the metagrain in this respect, which is stronger than the inelastic anisotropy of equiaxed single grains of constituent phases.

Elastic anisotropy degree is quantified using two measures proposed in Appendix B. It is concluded that the local anisotropy of constituent phases is not strong. Contrary to inelastic properties, the presence of different orientation variants of γ phase in the metagrain reduces its elastic anisotropy degree when comparing the elastic properties of single lamella. It is also concluded that, as far as overall elastic properties of untextured polycrystal of $\alpha_2 + \gamma$-TiAl are concerned, the difference between the Young modulus and the shear modulus predicted with use of the different variants of the modelling scheme is not substantial. The reason is the weak elastic anisotropy of the metagrain.

A. Homogenized properties of the lamellar metagrain

The overall compliance tensor of a metagrain $\mathbb{M}_{mc}$ and the overall eigenstrain $\boldsymbol{\varepsilon}^{res}_{mc}$ are obtained using Eqs. (2.7)-(2.11). They have the form (no summation convention):

$$\mathbb{M}^{LL}_{mc} = \{(\mathbb{M}^{LL}_i)^{-1}\}^{-1}, \tag{A.1}$$

$$\mathbb{M}^{LT}_{mc} = \{(\mathbb{M}^{LL}_i)^{-1}\}^{-1} \circ \{(\mathbb{M}^{LL}_i)^{-1} \circ \mathbb{M}^{LT}_i\}\ , \tag{A.2}$$

$$\mathbb{M}^{TL}_{mc} = \{\mathbb{M}^{TL}_i \circ (\mathbb{M}^{LL}_i)^{-1}\} \circ \{(\mathbb{M}^{LL}_i)^{-1}\}^{-1}, \tag{A.3}$$

$$\mathbb{M}^{TT}_{mc} = \{\mathbb{M}^{TT}_i - \mathbb{M}^{TL}_i \circ (\mathbb{M}^{LL}_i)^{-1} \circ \mathbb{M}^{LT}_i\} + \tag{A.4}$$

$$+\{\mathbb{M}^{TL}_i \circ (\mathbb{M}^{LL}_i)^{-1}\} \circ \{(\mathbb{M}^{LL}_i)^{-1}\}^{-1} \circ \{(\mathbb{M}^{LL}_i)^{-1} \circ \mathbb{M}^{LT}_i\}$$

$$\boldsymbol{\varepsilon}^{resL}_{mc} = \{\boldsymbol{\varepsilon}^{resL}_i\}\ , \tag{A.5}$$

$$\boldsymbol{\varepsilon}^{resT}_{mc} = \{\boldsymbol{\varepsilon}^{resT}_i\} + \{\mathbb{M}^{TL}_i \circ (\mathbb{M}^{LL}_i)^{-1} \cdot (\boldsymbol{\varepsilon}^{resL}_{mc} - \boldsymbol{\varepsilon}^{resL}_i)\}. \tag{A.6}$$

The following notation has been introduced above:

$$\mathbf{a}^L = \mathbb{P}^L \cdot \mathbf{a}, \quad \mathbf{a}^T = \mathbb{P}^T \cdot \mathbf{a}, \quad \mathbf{a}^L + \mathbf{a}^T = \mathbf{a}, \tag{A.7}$$

$$\mathbb{T}^{LL} = \mathbb{P}^L \circ \mathbb{T} \circ \mathbb{P}^L, \quad \mathbb{T}^{LT} = \mathbb{P}^L \circ \mathbb{T} \circ \mathbb{P}^T, \tag{A.8}$$

$$\mathbb{T}^{TL} = \mathbb{P}^T \circ \mathbb{T} \circ \mathbb{P}^L, \quad \mathbb{T}^{TT} = \mathbb{P}^T \circ \mathbb{T} \circ \mathbb{P}^T, \tag{A.9}$$

$$\mathbb{T} = \mathbb{T}^{LL} + \mathbb{T}^{LT} + \mathbb{T}^{TL} + \mathbb{T}^{TT}. \tag{A.10}$$

where $\mathbb{T}$ is any fourth order tensor and $\mathbf{a}$ is any second order tensor, $\mathbb{P}^L$, $\mathbb{P}^T$ are specified by (2.9). Note that the sign of inverse of a tensor $\mathbb{M}^{LL}$ in (A.1-A.6) denotes a partial inverse performed in the corresponding three-dimensional subspace.

Localization tensor $\mathbb{A}_i$ and concentration tensor $\mathbb{B}_i$ defined by Eq. (2.12) are specified as follows:

$$\begin{aligned}
&\mathbb{B}_{mc}^{LL} = (\mathbb{M}_i^{LL})^{-1} \circ \mathbb{M}_{mc}^{LL},\\
&\mathbb{B}_{mc}^{LT} = (\mathbb{M}_i^{LL})^{-1} \circ (\mathbb{M}_{mc}^{LT} - \mathbb{M}_i^{LT}),\\
&\mathbb{A}_{mc}^{TL} = (\mathbb{L}_i^{TT})^{-1} \circ (\mathbb{L}_{mc}^{TL} - \mathbb{L}_i^{TL}),\\
&\mathbb{A}_{mc}^{TT} = (\mathbb{L}_i^{TT})^{-1} \circ \mathbb{L}_{mc}^{TT},\\
&\mathbb{B}^{TL} = \mathbb{O}, \mathbb{B}^{TT} = \mathbb{P}^T, \mathbb{A}^{LT} = \mathbb{O}, \mathbb{A}^{LL} = \mathbb{P}^L
\end{aligned} \tag{A.11}$$

and

$$\begin{aligned}
&\boldsymbol{\alpha}_i^L = \mathbf{0}, \boldsymbol{\beta}_i^T = \mathbf{0},\\
&\boldsymbol{\alpha}_i^T = \boldsymbol{\varepsilon}_i^{\mathrm{res}T} - ((\mathbb{L}_i^{TT})^{-1} \circ \mathbb{L}_{mc}^{TT}) \cdot \boldsymbol{\varepsilon}_{mc}^{\mathrm{res}T} -\\
&\quad (\mathbb{L}_i^{TT})^{-1} \cdot (\mathbb{L}_{mc}^{TL} \cdot \boldsymbol{\varepsilon}_{mc}^{\mathrm{res}L} - \mathbb{L}_i^{TL} \cdot \boldsymbol{\varepsilon}_i^{\mathrm{res}L}),\\
&\boldsymbol{\beta}_i^L = (\mathbb{M}_i^{LL})^{-1} \cdot (\boldsymbol{\varepsilon}_{mc}^{\mathrm{res}L} - \boldsymbol{\varepsilon}_i^{\mathrm{res}L}),
\end{aligned} \tag{A.12}$$

where $\mathbb{O}$ is the IV-th order tensor of all components equal to zero.

B Measures of anisotropy

There is no unique measure of anisotropy degree of the properties described by the the fourth order tensor with symmetries of elasticity tensor [26, 27]. In this work two such measures are proposed.

First measure of anisotropy generalizes the Zener parameter proposed for cubic materials [44] and is well suited for the volumetrically isotropic materials [4, 15]. Let h_K and $\boldsymbol{\omega}_K$ denote Kelvin moduli and corresponding eigenstates of the stiffness tensor, i.e.:

$$\mathbb{L} = \sum_{K=I}^{VI} h_K \boldsymbol{\omega}_K \otimes \boldsymbol{\omega}_K$$

ordered according to the rule

$$K > L \Leftrightarrow (\mathrm{tr}\boldsymbol{\omega}_K)^2 \geqslant (\mathrm{tr}\boldsymbol{\omega}_L)^2 .$$

We say that the anisotropy of $\mathbb{L}$ is the stronger the higher is the value of the following ratio

$$\begin{aligned}
&\zeta = \left| \ln \left(\frac{h_{\min}^D}{h_{\max}^D} \right) \right|, \quad h_{\min}^D = \min_{K=I,...,V} (h_K),\\
&h_{\max}^D = \max_{K=I,...,V} (h_K).
\end{aligned} \tag{B.1}$$

For isotropic materials the value of ζ is zero. Note that the original Zener parameter for cubic materials reads

$$\zeta_{Zener} = \frac{L_{1111} - L_{1122}}{2L_{1212}} = \frac{h_{IV,V}}{h_{I,II,III}}$$

and is equivalent to the ratio of two distinct deviatoric Kelvin moduli obtained by spectral decomposition of elasticity tensor for these materials. The logarithmic function has been used in the definition (B.1) in order to obtain the same value of these parameter for $\mathbb{L}$ and its inverse $\mathbb{M} = \mathbb{L}^{-1}$. The main drawback of the above indicator of anisotropy degree is that, it is equal to zero not only for isotropic materials, e.g. ζ =0 in the case of anisotropic material for which $h_{VI} \neq h_K = h_J$ for any pair $K, J = I, ..., V$ while $(\mathrm{tr}\boldsymbol{\omega}_{VI})^2 \neq 3$. The forms of the spectral decompositions for all symmetry groups of Hooke's tensor have been provided in [16]. The reader is referred to this publication for the details concerning the form of eigenstates as well as the dependencies of Kelvin moduli and stiffness distributors on the independent components of $\mathbb{L}$ for the crystal symmetries appearing in this article. The notation used in the present paper is consistent with the one in [16].

The second measure of anisotropy uses the harmonic decomposition of the stiffness tensor into its isotropic and anisotropic part [29, 30]. The isotropic part of the tensor $\mathbb{L}$ is defined as

$$\mathbb{L}^{iso} = h_P \mathbb{I}_P + h_D \mathbb{I}_D, \quad \mathbb{I}_P = \frac{1}{3} \mathbf{I} \otimes \mathbf{I}, \quad \mathbb{I}_D = \mathbb{I}^S - \mathbb{I}_P,$$

where $\mathbf{I}$ is the second order identity tensor and

$$\begin{aligned}
&h_P = \tfrac{1}{3} \mathbf{I} \cdot \mathbb{L} \cdot \mathbf{I} = \tfrac{1}{3} L_{iijj},\\
&h_D = \tfrac{1}{5} \left(\mathbb{I}^S \cdot \mathbb{L} - h_P \right) = \tfrac{1}{5} \left(L_{ijij} - h_P \right).
\end{aligned}$$

The anisotropic part is $\mathbb{L}^{ani} = \mathbb{L} - \mathbb{L}^{iso}$. Now, we say that the anisotropy of $\mathbb{L}$ is the stronger the higher is the value of the following ratio

$$\chi = \frac{\left\| (\ln \mathbb{L})^{ani} \right\|}{\|\ln \mathbb{L}\|}, \qquad 0 \leqslant \chi < 1, \tag{B.2}$$

where

$$\ln \mathbb{L} = \sum_{K=I}^{VI} (\ln h_K)\, \omega_K \otimes \omega_K, \quad \|\mathbb{T}\| = T_{ijkl} T_{ijkl}.$$

For isotropic materials, and only for such materials, the value of the above parameter is zero. The parameter χ is always less than one because the stiffness tensor is positive definite. The tensor function ln $\mathbb{L}$ is used to ensure the same value of measure χ for $\mathbb{L}$ and its inverse $\mathbb{M}$. When introducing this measure we have been inspired by the work [18] where alternative definitions of a norm and a metric for the set of the stiffness tensors have been proposed.

Acknowledgements

The work was partly supported by the Ministry of Science and Higher Education of Poland in the framework of the research projects N N501 068135.

REFERENCES

[1] F. Appel, R. Wagner, Microstructure and deformation of two-phase γ-titanium aluminides. Mater. Sci. Eng R. **22**, 187-268 (1998).

[2] J.G. Berryman, Bounds and estimates for elastic constants of random polycrystals of laminates. Int. J. Solids Structures **42**, 3730-3743 (2005).

[3] R. Brenner, R.A. Lebensohn, O. Castelnau, Elastic anisotropy and yield surface estimates of polycrystals. Int. J. Solids Structures **46**, 3018-3026 (2009).

[4] W.T. Burzynski, Studium nad hipotezami wytezenia. Lwów, 1928. (także Dzieła Wybrane, t. I, PWN, Warszawa 1982).

[5] A. El Omri, A. Fennan, F. Sidoroff, A. Hihi, Elastic-plastic homogenization for layered composites. Eur. J. Mech. A/Solids **19**, 585-601 (2000).

[6] J.D. Eshelby, The determination of the elastic field of an ellipsoidal inclusion, and related problems. Proc. Roy. Soc. A **241**, 376-396 (1957).

[7] R. Hill, Continuum micro-mechanics of elastoplastic polycrystals. J. Mech. Phys. Solids **13**, 89-101 (1965).

[8] J.W. Hutchinson, Elastic-plastic behavior of polycrystalline metals and composites. Proc. Roy. Soc. London **A319**, 247-272 (1970).

[9] K. Kishida, H. Inui, M. Yamaguchi, Deformation of PST crystals of a TiAl/Ti_3Al two-phase alloy at 1000°C. Intermetallics **7**, 1131-1139 (1999).

[10] U.F. Kocks, H. Chandra, Slip geometry in partially constrained deformation. Acta Metall. **30**, 695 (1982).

[11] Y. Koizumi, T. Nakano, Y. Umakoshi, Plastic deformation and fracture behaviour of Ti_3Al single crystals deformed at high temperature under cyclic loading. Acta Mater. **47**, 2019-2029 (1999).

[12] K. Kowalczyk, J. Ostrowska-Maciejewska, Energy-based limit conditions for transversally isotropic solids. Arch. Mech. **54**(5-6), 497-523 (2002).

[13] K. Kowalczyk-Gajewska, Bounds and self-consistent estimates of overall properties for random polycrystals described by linear constitutive laws. Arch. Mech. **61**(6), 475-503 (2009).

[14] K. Kowalczyk-Gajewska, Micromechanical modelling of metals and alloys of high specific strength, IFTR Reports 1/2011 (2011).

[15] K. Kowalczyk-Gajewska, J. Ostrowska-Maciejewska, The influence of internal restrictions on the elastic properties of anisotropic materials. Arch. Mech **56**, 205-232 (2004).

[16] K. Kowalczyk-Gajewska, J. Ostrowska-Maciejewska, Review on spectral decomposition of Hooke's tensor for all symmetry groups of linear elastic material. Enging. Trans. **57**, 145-183 (2009).

[17] R.A. Lebensohn, H. Uhlenhut, C. Hartig, H. Mecking, Plastic flow of γ-TiAl-based polysynthetically twinned crystals: micromechanical modelling and experimental validation. Acta Mater. **46**, 229-236 (1998).

[18] M. Moakher, N. Norris, The closest elastic tensor of arbitrary symmetry to an elasticity tensor of lower symmetry. J. Elasticity **85**, 215-263 (2006).

[19] T. Nakano, B. Ogawa, Y. Koizumi, Y. Umakoshi, Plastic deformation behaviour and dislocation structure in Ti_3Al single crystals cyclically deforming by prism slip. Acta Mater. **46**, 4311-4324 (1998).

[20] S. Nemat-Nasser, M. Hori, Micromechanics: overall properties of heterogeneous materials. North-Holland Elsevier, 1999.

[21] S. Nikolov, R.A. Lebensohn, D. Raabe, Self-consistent modeling of large plastic deformation, texture and morphology evolution in semi-crystalline polymers. J. Mech. Phys. Solids **54**, 1350-1375 (2006).

[22] J. Ostrowska-Maciejewska, J. Rychlewski, Generalized proper states for anisotropic elastic materials. Arch. Mech. **53**(4-5), 501-518 (2001).

[23] V. Paidar, M. Yamaguchi, Constrained deformation of a lamellar structure. Mater. Sci. Engng A **462**, 460-464 (2007).

[24] H. Petryk, General conditions for uniqueness in materials with multiple mechanisms of inelastic deformation. J. Phys. Mech. Solids **48**, 367-396 (2000).

[25] A. Roos, J.-L. Chaboche, L. Gelebart, J. Crepin, Multiscale modelling of titanium aluminides. Int. J. Plasticity **20**, 811-830 (2004).

[26] J. Rychlewski, Zur Abschätzung der Anisotropie. ZAMM **65**, 256-258 (1985).

[27] J. Rychlewski, Anisotropy degree of elastic materials. Arch. Mech. **41**, 697-715 (1989).

[28] J. Rychlewski, Unconventional approach to linear elasticity. Arch. Mech. **47**(2), 149-171 (1995).

[29] J. Rychlewski, A qualitative approach to Hooke's tensors. Part I. Arch. Mech. **52**, 737-759 (2000).

[30] J. Rychlewski, A qualitative approach to Hooke's tensors. Part II. Arch. Mech. **53**, 45-63 (2001).

[31] S. Stupkiewicz, H. Petryk, Modelling of laminated microstractures in stress-induced martensitic transformations. J. Phys. Mech. Solids **50**, 2303-2331 (2002).

[32] S. Stupkiewicz, H. Petryk, A bi-crystal aggregate model of pseudoelastic behaviour of shape-memory alloy polycrystals. Int. J. Mech. Sci. **52**, 219-228 (2010).

[33] M.S. Szczerba, T. Bajor, T. Tokarski, Is there a critical resolved shear stress for twinning in face-centered cubic crystals? Phil. Mag. **84**, 481-502 (2004).

[34] K. Tanaka, Single-crystal elastic constants of γ-TiAl. Phil. Mag. Lett. **73**, 71-78 (1996).

[35] K. Tanaka, K. Okamoto, H. Inui, Y. Minonishi, M. Yamaguchi, M. Koiwa, Elastic constants and their temperature dependence for the intermetallic compound Ti_3Al. Phil. Mag. A **73**, 1475-1488 (1996).

[36] P. Van Houtte, On the equivalence of the relaxed Taylor theory and the Bishop-Hill theory for partially constrained plastic deformation of crystal. Mater. Sci. Eng. **55**, 69-77 (1982).

[37] P. Van Houtte, L. Delannay, I. Samajdar, Quantitative prediction of cold rolling textures in low carbon steel by means of the LAMEL model. Textures and Microtextures **31**, 109-149 (1999).

[38] P. Van Houtte, S. Li, M. Seefeldt, L. Delannay, Deformation texture prediction: from the Taylor model to the advanced Lamel model. Int. J. Plasticity **21**, 589-624 (2005).

[39] L.J. Walpole, Advances in Applied Mechanics, volume 21, chapter Elastic Behavior of Composite Metarials: Theoretical Foundations, pages 169-236 (1981).

[40] M. Werwer, A. Cornec, Numerical simulation of plastic deformation and fracture in polysynthetically twinned (PST) crystals of TiAl. Comput. Mater. Sci. **19**, 97-107 (2000).

[41] M. Werwer, A. Cornec, The role of superdislocations for modeling plastic deformation of lamellar TiAl. Int. J. Plasticity **22**, 1683-1698 (2006).

[42] M. Werwer, R. Kabir, A. Cornec, K.-H. Schwalbe, Fracture in lamellar TiAl simulated with the cohesive model. Engng. Fracture Mech. **74**, 2615-2638 (2007).

[43] J.R. Willis, Advances in Applied Mechanics, volume 21, chapter Variational and Related Methods for the Overall Properties of Composites, pages 2-79 (1981).

[44] C. Zener, Elasticite et Anelasticite des Metaux. Dunod, Paris, 1955.

Received: 10 January 2011.